Wavevector dependence of population and spin dynamics of exciton polaritons in bulk semiconductors

2006 J. Phys.: Condens. Matter 18 315

(http://iopscience.iop.org/0953-8984/18/1/023)

INSTITUTE OF PHYSICS PUBLISHING JOURNAL OF PHYSICS: CONDENSED MATTER

J. Phys.: Condens. Matter **18** (2006) 315–331 doi:10.1088/0953-8984/18/1/023

Wavevector dependence of population and spin dynamics of exciton polaritons in bulk semiconductors

S Cronenberger, H Rahimpour Soleimani[1], T Ostatnický[2], O Crégut, M Gallart, P Gilliot and B Hönerlage

IPCMS/GONLO, UMR 7504 CNRS-ULP, BP 43, 23, rue du Lœss, F-67034 Strasbourg CEDEX 2, France

Received 20 September 2005, in final form 30 October 2005
Published 9 December 2005
Online at stacks.iop.org/JPhysCM/18/315

Abstract

We study the dynamics of a system consisting of exciton polaritons and biexcitons in bulk semiconductors. The polariton dispersion curve is scanned in a pump-and-probe experiment by looking at different excitation and detection wavelengths. This allows us to determine the influence of the polariton wavevector on polariton-spin relaxation processes and on their overall population dynamics. We perform these studies at low temperatures in bulk CuCl samples on a sub-picosecond timescale. We evaluate how the optical properties close to the exciton resonance develop with time from induced absorption to gain, depending on the wavelength and the intensity of excitation. This allows us to determine the polariton- and biexciton-population relaxation dynamics inside the bottleneck spectral region, and their spin dynamics, and reveals the importance of scattering and propagation effects.

(Some figures in this article are in colour only in the electronic version)

1. Introduction

In semiconductors, within the framework of kp perturbation theory, the eigenvalues of the electron momentum k, of the total angular momentum operator j, and of j_z are good quantum numbers for defining the electron states, since the electron Hamiltonian is supposed to commute with these operators. Beyond this first approximation, additional terms have to be added to the zero-order Hamiltonian, which are due to spin–orbit coupling and electron–hole exchange interaction. They result in a coupling between k and j. Electrons and holes optically excited in states characterized by a well defined pseudo-spin state (i.e. with total angular momentum j and j_z) will suffer relaxation processes associated to the transitions between these states. These relaxations will be strongly determined by processes inducing variations of the electron

[1] Permanent address: Department of Physics, University of Guilan, PO Box 1914, Rasht, Iran.
[2] Permanent address: Department of Chemical Physics, Charles University, Ke Karlovu 3, 12116 Prague 2, Czech Republic.

momentum. They will thus depend on the mean value of the k vector and vary along the dispersion curve of the quasi-particles which are excited in the crystal.

Excitons are the lowest lying electronic excitations in intrinsic semiconductors. They can be described as a bound state of an electron in the conduction band and a hole in a valence band, interacting via Coulomb interaction. Excitons are considered as quasi-particles: they have a wavevector-dependent energy and possess an internal structure, characterized by their total angular momentum (or pseudo-spin) which combines the individual electron and hole pseudo-spins. Dispersion, internal structure, and resulting residual (exchange) interactions are mainly determined by the crystal symmetry and the one-particle band structure. Within the quasiparticle concept, different relaxation processes are possible: energy relaxation due to inelastic scattering, change of the wavevector due to elastic or inelastic scattering, and change of the spin state if the internal structure of the exciton changes with time. Spin-relaxation times are in general longer than optical coherence times and comparable to population lifetimes. It is important to understand the spin and energy relaxation dynamics since the quasi-particles can carry and store information on quite long timescales [1–4]. We have shown in a previous paper [5] how the dynamics of excitons can be determined through induced absorption to biexcitons in non-degenerate pump-and-probe experiments.

In that previous publication [5], a pump-and-probe induced absorption experiment is interpreted in a scheme involving ground, exciton and biexciton states in order to measure the exciton spin relaxation. Leaving this four-level scheme, which is an oversimplified basis, the present paper is based on the fact that, in our experiments, the quasi-particles which are excited are not excitons with (quasi-) discrete photon energies but polaritons which have a continuous spectrum. As also observed in microcavities, polaritons and their spins have dynamics which depend strongly on the respective weight of the exciton and photon parts in the polariton wavefunction. This dependence can be probed when scanning the photon energies from polaritons which have pure photon character, i.e. energies far below the excitonic resonance, to polaritons with a strong exciton character close to the resonance. The population and spin dynamics is not only determined by this balance between the photon- and exciton-characters: even for polaritons which are exciton-like, the polariton effect induces very fast changes of the group velocity with energy, which has strong effects on the collision rate of a polariton with the other quasi-particles or the crystal defects. Such strong interactions between exciton-like polaritons lead moreover to the formation of a biexciton population which, in turn, strongly influences the polariton spin dynamics when they decay back into exciton–polaritons. The polariton dynamics and their spin dynamics are thus strongly determined by their propagation and their study can then give valuable information about the spin transport in semiconductor structures.

Our present paper is thus aimed at emphasizing this wavevector dependence of the spin-polarized polariton dynamics in CuCl and at giving a comprehensive study of the full polariton, longitudinal exciton, and biexciton dynamics and of their spin. Copper chloride is an ideal compound for this type of study, as it has a very simple valence band structure and shows very large exciton and biexciton binding energies.

To fit and explain our experimental data, we use a model which takes into account not only the spin dynamics of the polaritons, but also a full description of the polariton population dynamics, including their population transfer to the biexciton state and non-radiative longitudinal exciton levels. The rate equations governing the biexciton–polariton system in CuCl are based on a now long set of experiences and publications. Femtosecond pulses have already been used to explore the coherent dynamics of the polaritons and bipolaritons in bulk CdS [6] using four-wave mixing techniques. The novelty of the results we present here

rests on the new interest for the spin dynamics and on the use of femtosecond pulses to study such populations and spin dynamics of propagating polaritons.

2. Bases on exciton polaritons in copper chloride

Copper chloride is a highly ionic I–VII semiconductor compound with zinc blende structure. It has a direct band gap at the centre of the Brillouin zone. Its lowest conduction band (Γ_6 symmetry) is only spin degenerate. At the Γ point, spin–orbit coupling splits the highest valence bands into a fourfold degenerate band with Γ_8 symmetry and a twofold degenerate band with Γ_7 symmetry. In contrast to most other semiconductors with the zinc blende structure, the uppermost valence band in CuCl is the one with Γ_7 symmetry. The split-off band is about 81 meV lower in energy. Therefore, the exciton ground state is only fourfold degenerate with a binding energy of about 197 meV at 4 K [7–12]. The resulting excitons transform like Γ_2 and Γ_5, respectively. The triplet Γ_2 exciton state has an energy of $E_{\mathrm{Tri}} = 3.2000$ eV at 4 K and does not carry a dipole moment. The Γ_5 exciton state consists of two transverse excitons, which are dipole active, and a longitudinal exciton. Due to the analytical and the non-analytical exchange interactions, the degeneracy of the exciton ground state is partially lifted. While the energy of the triplet exciton remains unchanged, the energies of the transverse excitons and of the longitudinal one increase to $E_{\mathrm{T}} = 3.2025$ eV and $E_{\mathrm{L}} = 3.2080$ eV [13], respectively. The dipole active transverse excitons couple strongly to the light field, giving rise to exciton polaritons as propagating modes. These polaritons may be constructed in a basis of linear or circular polarizations with right or left helicities designed by σ^+ or σ^-. In a simple one-oscillator model, the polariton dispersion is characterized by the longitudinal and transverse exciton energies, the background electric constant $\varepsilon_{\mathrm{b}} = 5$ and the effective exciton mass $M_{\mathrm{X}} = 2.5\, m_0$, where m_0 is the electron mass [13]. The dispersion relation and the group velocity of the polaritons can be determined using the simple one-oscillator model, which properly applies to CuCl. The dispersion relation is given by [12]

$$\frac{\hbar^2 Q^2}{E_i(Q)} = \varepsilon_{\mathrm{b}}\left(1 + \frac{4\pi\beta E_{\mathrm{T}}^2(Q=0)}{E_{\mathrm{T}}^2(Q) - E_i^2(Q)}\right) \tag{1}$$

where the oscillator strength $4\pi\beta$ can be expressed in terms of the non-analytical exchange interaction giving rise to the longitudinal transverse splitting:

$$4\pi\beta = \frac{E_{\mathrm{L}}^2(Q=0) - E_{\mathrm{T}}^2(Q=0)}{E_{\mathrm{T}}^2(Q=0)}.$$

Two excitons can couple and form exciton molecules [14, 15]. Their properties have been largely investigated using time-resolved pump-and-probe [16–19] or luminescence [20–25] experiments. In CuCl, the biexciton ground state energy, $E_{\mathrm{Bi}} = 6.3720$ eV at 4 K, corresponds to an important biexciton binding energy ($E_{\mathrm{b}} = 28$ meV) when compared to the threshold of the two-exciton continuum. The biexciton ground state is non-degenerate and has Γ_1 symmetry. Its energy and symmetry have been identified by non-degenerate two-photon absorption involving only polaritons from the lower branch. Other biexciton states which could exist [26] have not been found in CuCl. Time-resolved four-wave mixing experiments close to the biexciton resonance show a free induction decay of the signal and no photon echo. Therefore one can conclude that the lines involving biexcitons are mainly homogeneously broadened. The linewidth of the transition of about 0.03–0.1 meV [27–29] depends on the excitation intensity. No indications for an inhomogeneous broadening were observed in bulk material [30]. A detailed study of the two-photon absorption line shape showing the importance of the upper polariton states and that of the bipolariton model when compared to the giant oscillator strength model are beyond the scope of this paper [28–33]. The biexciton dispersion is characterized by roughly twice the exciton effective mass $M_{\mathrm{Bi}} = 5\, m_0$.

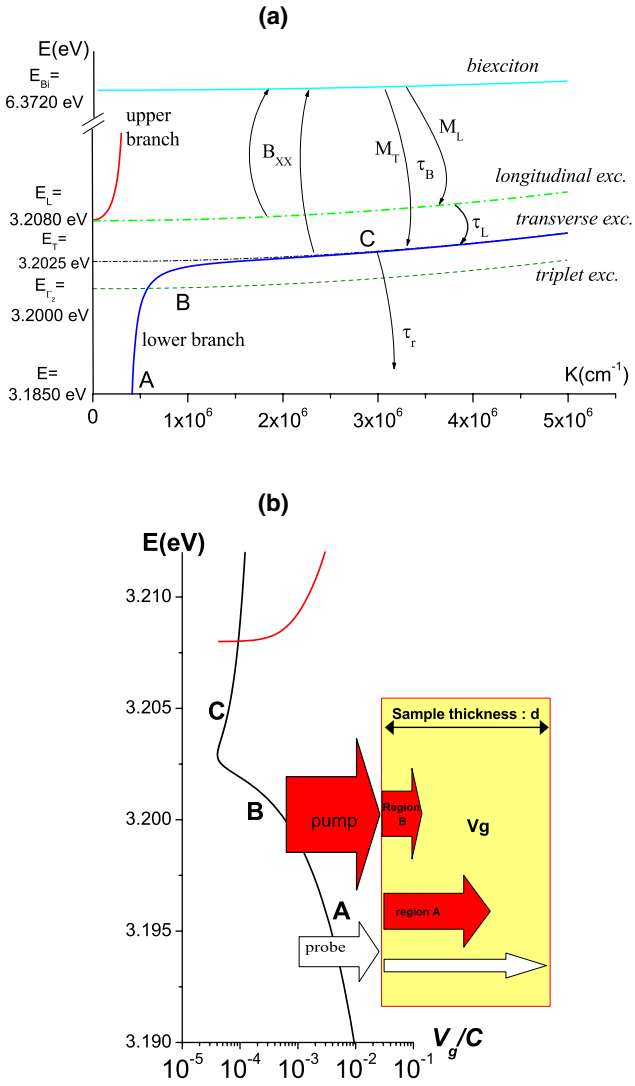

Figure 1. (a) Polariton dispersion $E(K)$ in the vicinity of the bottleneck region calculated from the parameters of CuCl using the one-oscillator model. A, B, and C denote the region of fast ballistic polaritons, the spin-flip region, and the bottleneck region, respectively (see text). N_i and τ_i denote different relaxation times and B_{XX} the probability of biexciton formation (see text). (b) Polariton group velocity calculated from their dispersion using the parameters given in the text.

Biexcitons may be excited from the crystal ground state either by two polaritons of parallel linear polarization or from two circularly polarized polaritons of opposite helicity. This absorption process can be performed either simultaneously as in a two-photon absorption or in a two-step process where first a population of polaritons of a well defined helicity and energy is created. It is then probed by absorption of polaritons from a second pulse which induces the transition to the biexciton state obeying energy and momentum conservation. It is important to stress that, at finite wavevector, this selection rule is only valid for polaritons which are propagating in the same direction [33]. We will concentrate here on this second process, which is schematically indicated in figure 1, together with the dispersion relation and

the group velocity of the polaritons. If E_p denotes the photon energy of polaritons created by the pump beam and E_t that from the probe beam, energy conservation implies that

$$E_p(K_p) + E_t(K_t) = E_{Bi}(K_p + K_t). \tag{2}$$

We will make full use of equations (1) and (2) throughout the analysis of our results. This paper is organized as follows: a brief description of the experimental conditions is given in section 3, followed by a presentation of the experimental results (section 4), and a discussion and modelling of these results in section 5.

3. Experimental details

We study freestanding CuCl platelets, which were grown by vapour phase transport in a closed tube containing H_2 and CuCl powder [10]. From studying the interference of reflection from front and rear surfaces, our samples turn out to be quite inhomogeneous in thickness with a mean value of about 20 μm. The samples are placed inside a cold-finger cryostat whose temperature can be varied between 4 and 100 K. The experimental set-up and the situation of excitation and detection are sketched in figures 2 and 3, respectively: spectrally broad femtosecond pulses from a self mode-locked Ti:sapphire laser are amplified in a regenerative amplifier and then frequency doubled using a BBO crystal. At low sample temperatures, the frequency of the laser pulses is centred on 3.208 eV with a full width at half maximum (FWHM) of about 15 meV. As shown in figure 3, the excitation entirely covers the exciton resonance. When increasing the temperature, the photon energy of the central frequency of the laser is changed in order to follow the exciton resonance, which shifts towards higher photon energies in CuCl. The pulses pass an optical delay line and a linear polarizer, followed by a $\lambda/4$ plate. They are circularly polarized with σ^+ helicity. The pump beam is focused onto the sample surface into a spot of about 100 μm in diameter. A beam splitter separates a small part from the amplified laser emission and a probe beam is generated using a second BBO crystal for frequency doubling. The probe also has a spectral width of 15 meV (FWHM) and is centred at the spectral position of the induced absorption band of the exciton–biexciton transition, which is situated around 3.1695 eV at 4 K (see figure 3). The linearly polarized light then passes successively a $\lambda/2$ plate and the $\lambda/4$ plate mentioned above. Using the same lens as for the pump beam, the probe is focused onto the surface of the CuCl crystal into the spot excited by the pump beam. If the linear polarization of the probe is parallel to the neutral axis of the $\lambda/2$ plate, the probe beam is circularly polarized with σ^+ helicity on the surface of the sample. By rotating the $\lambda/2$ plate, circularly polarized light with σ^- helicity is obtained behind the $\lambda/4$ plate. Care is taken that the rotation of the $\lambda/2$ plate does not influence the spatial coincidence of the two spots, which is controlled by a video camera. The probe and pump pulses have durations of 170 fs. They propagate almost collinearly along the [111] direction inside the sample. The probe beam, transmitted through the sample, is carefully spatially filtered by a diaphragm and is then analysed time-integrated but spectrally resolved by a spectrometer and a cooled CCD camera.

We measure the intensity of the probe pulse when transmitted through the sample separately without excitation by the pump pulse (noted I_T) and with pump-pulse excitation at a time delay t between the pulses (denoted $I_T^L(t)$). In addition, we determine the time-integrated sample emission and the diffused light I_{Str} which are due to the pump-pulse excitation alone. We subtract I_{Str} from $I_T^L(t)$ and obtain the induced change of the transmitted intensity by

$$I_{ind}(t) = I_T^L(t) - I_{Str} - I_T.$$

We then calculate the induced transmission change

$$\Delta T(t) = I_{ind}(t)/I_T.$$

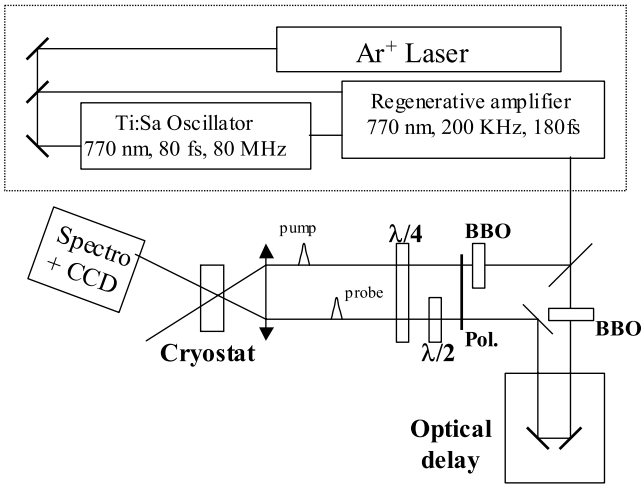

Figure 2. Experimental set-up.

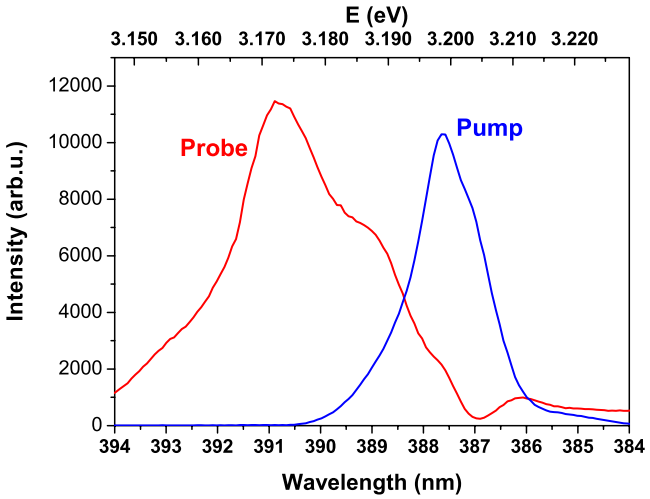

Figure 3. Spectral position and shape of the pump and the probe pulses.

ΔT is negative if the probe pulse is subject to induced absorption and positive if the absorption is bleached or if the pulse is amplified due to optical gain at the photon energy considered. Then, the induced probe-beam transmission is analysed as function of time delay t between the two incident pulses for both polarization sequences $\sigma^+\sigma^+$ and $\sigma^+\sigma^-$. The resulting induced transmission changes for the $\sigma^+\sigma^+$ and the $\sigma^+\sigma^-$ configurations are denoted $\Delta T^{++}(t)$ and $\Delta T^{+-}(t)$, respectively. The measurements were performed for different excitation intensities and sample temperatures. The overall temporal resolution is about 0.3 ps and the spectral resolution 0.6 meV.

4. Experimental results

The induced transmission changes measure the probability that polaritons created by the pump pulse at a given photon energy with σ^+ helicity undergo a transition to biexcitons by absorption

of a polariton from the probe pulse. For collinearly propagating polaritons, due to the selection rules, this is only possible if the probe pulse has σ^- helicity. If, however, polaritons from the pump pulse perform a spin-flip to σ^- helicity, their transition to the biexciton state can be induced with polaritons from a probe pulse with σ^+ helicity. It is interesting to notice that such spin-flip processes occur if the direction of propagation of the polaritons or their internal spin structure change due to a collision process. Collisions can be due to interactions with crystal defects or with acoustical or optical phonons. Collisions with optical phonons are very unlikely since we are working mainly at 4 K. In addition to these processes, polariton–polariton scattering and exchange interactions between the electrons and holes may lead to spin relaxation.

Besides an induced absorption, polaritons from the probe pulse may also induce the recombination of biexcitons if such a population is already present. This process shows up as optical amplification if there is a population inversion between biexcitons and longitudinal excitons or polaritons.

As discussed in more detail in [5], the polaritons have a group velocity and a density of states which depend strongly on their photon energy. They are therefore influenced in different ways by surface effects, lattice defects, scattering with phonons or other excitons or polaritons. The competition between the scattering processes leads to different gain and induced absorption dynamics, which are characteristic for the spectral regions tested by the probe beam. They are denoted A, B, C-I, and C-II in the following and are indicated schematically in figure 1.

Let us discuss the absorption and emission dynamics of a sample for the following experimental conditions: the pump pulses cover spectrally the exciton resonance and extend in their wings down to the region covered by the probe pulse, as shown in figure 3. Biexciton formation is possible in CuCl by coupling of two exciton polaritons. They may emit a longitudinal optical phonon whose energy $\hbar\omega_{\mathrm{LO}} = 26.0$ meV [10] is close to the biexciton binding energy ($E_{\mathrm{b}} = 28$ meV). This process is very efficient because of its nearly resonant nature and because of the highly polar binding of CuCl, leading to a strong coupling between electrons and longitudinal optical phonon. Biexcitons are thus created with a big wavevector and an excess kinetic energy of several meV. They may further thermalize on their dispersion curve by emission of acoustic phonons before they recombine radiatively. In this process, a photon-like polariton is generated together with a longitudinal exciton or a second, exciton-like polariton. The recombination obeys energy and momentum conservation. As indicated schematically in figure 1, this process gives rise to the M_{T} and M_{L} biexciton emission lines. The longitudinal excitons or polaritons can further thermalize to lower branch polaritons by emission of acoustic or optical phonons. In addition, two excitons or exciton polaritons may couple and again form biexcitons which relax their energy as described above.

Figures 4(a) and (b) give the spectrally and temporally resolved transmission changes $\Delta T/T$ in a contour plot for the $\sigma^+\sigma^-$ and the $\sigma^+\sigma^+$ configuration. The integrated intensity of pump pulses is 2.66 mJ/cm^2/pulse. This corresponds to an excitation of a maximum density of 5.2×10^{15} exciton polaritons/cm^2/pump pulse. In figure 4, the different grey values represent a linear scale of $\Delta T/T$ between -0.15 (black, corresponding to induced absorption) and +0.1 (white, due to bleaching of absorption or optical gain). In order to facilitate the interpretation of the differential transmission spectra we give also the time-integrated photoluminescence (PL) of the sample. The polarizations of the PL spectra are not resolved. In the contour plots, the black or white regions surrounded by white or black lines indicate the part where the signal is saturated on the given grey scale. As we will see, we attribute the evolution of the spectra to energy relaxation and polariton propagation.

Let us start with the positive transmission changes around 3.186 eV in figure 4(b) for the $\sigma^+\sigma^+$ configuration which is almost absent in figure 4(a). In our opinion this is due to

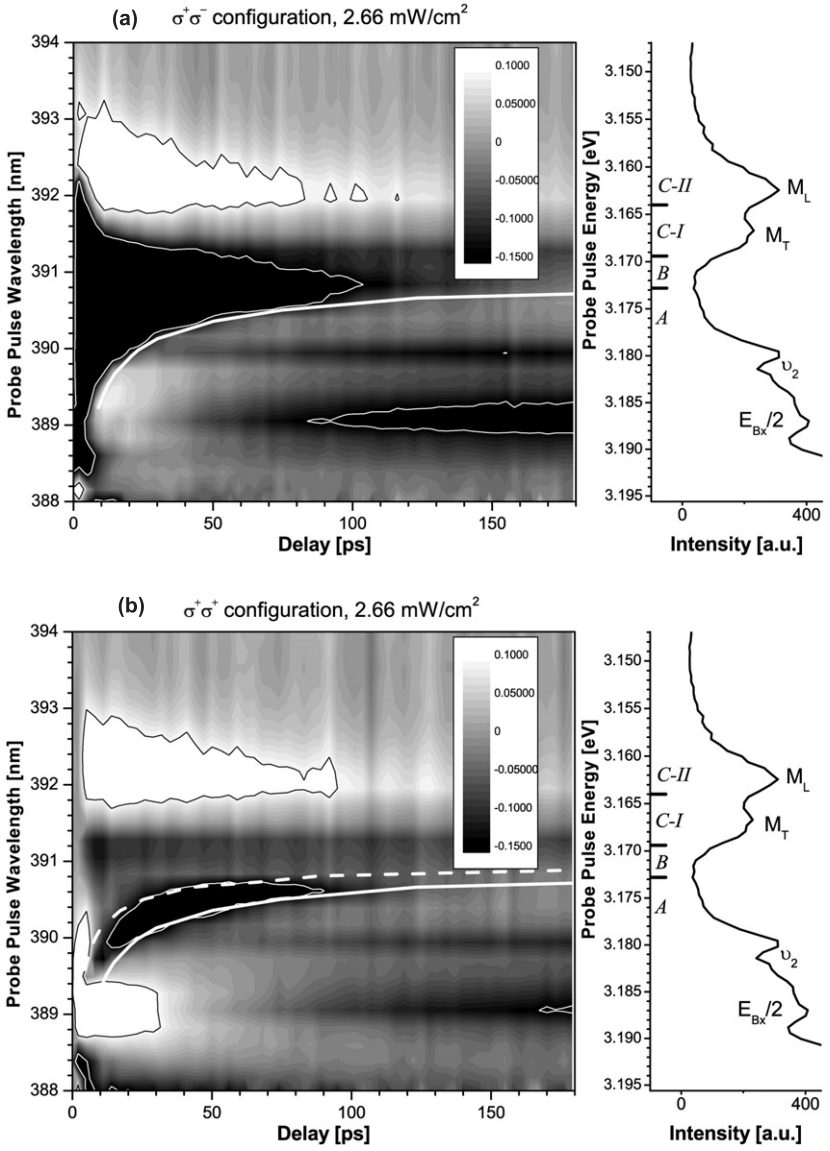

Figure 4. Contour diagram at 2.66 mJ/cm^2/pulse for (a) the $\sigma^+\sigma^-$ configuration and (b) for the $\sigma^+\sigma^+$ configuration.

a bleaching of the absorption induced by the wings of the pump pulse. As seen in the PL spectrum, the corresponding states are observed in emission. Positive transmission changes are also observed in the region of the M_{L} biexciton emission (3.161 eV). They are similar in the $\sigma^+\sigma^-$ and the $\sigma^+\sigma^+$ configurations. We attribute them to stimulated emission processes, which are induced by the probe beam polaritons from biexcitons to longitudinal excitons. The latter thermalize rapidly to lower polaritons, giving rise to a population inversion between biexcitons and longitudinal excitons. The strong stimulated emission ends after about 100 ps, the time at which the lines labelled ν_2 (around 3.179 eV) and at 3.186 eV appear. The line labelled ν_2 is

attributed in the literature to an exciton, bound to a neutral acceptor. It shows up in emission and absorption [34]. The energy difference between this line and the exciton polariton population around 3.205 eV, which is created by the pump pulse through strong linear absorption as well as through biexciton decay, corresponds to the energy of a longitudinal optical phonon. Therefore, we believe that the states around 3.179 eV are populated by a phonon replica of the exciton-like polaritons. The line close to 3.186 eV (which coincides with half the biexciton energy) has a similar origin: longitudinal excitons created by the recombination of biexcitons at 3.212 eV emit an optical phonon and are reabsorbed together with photons from the test beam to create biexcitons again. Both channels of phonon emission are in competition with the biexciton creation by two exciton-like polariton or an exciton polariton with a longitudinal exciton. Therefore, the phonon emission channels only become important at low exciton densities, i.e. after the end of the stimulated emission.

The different scattering processes involving biexciton recombination are not sensitive to the spin state of the exciton polaritons and there is no spin memory [35]. Between 3.165 and 3.195 eV and depending on the delay between probe and pump pulses, however, we observe a spin dependence. It is closely related to the propagation of the exciton polaritons: as indicated in figure 1(b), the polariton group velocity depends strongly on their photon energy. The full line in figure 4(a) gives the time which a ballistic polariton needs to run through a distance of 35 μm. In figure 4(b) a similar line is in addition given for 12 μm. For photon energies between 3.175 and 3.185 eV, figure 4(b) shows that the spin-flip from the σ^+ state to the σ^- state is maximum after the polaritons have propagated through about 20 μm and then drastically drops. The transfer rate is almost independent of the time of propagation. When having propagated over distances longer than 35 μm the spin memory is lost in both configurations. We have interpreted this result in [5] as being due to the fact that the polaritons hit the rear surface of the sample at different times, depending on their photon energy and therefore their group velocity. There, they are either transmitted as photons or they are reflected back into the sample. In the latter case, they can still give rise to induced absorption but their spin memory is lost. This is perhaps due to the poor surface quality of the samples. As discussed in the introduction, this is corroborated by the fact that the modulation of the interference fringes observed in transmission is only weak.

We can conclude from figure 4(b) that mainly sample defects lead to spin dephasing at 4 K: the number of collisions of polaritons with defects is only a function of the distance through which the polaritons have propagated, not of time. The number of collisions with phonons would on the contrary increase with time, which is not observed here.

For photon energies roughly between 3.173 and 3.171 eV the group velocity of the lower polaritons is so small that they do not reach the rear surface of the sample within 180 ps. We call this region the 'spin-flip region'. Here, and in the spectral region of the M_T line, the spin memory is conserved over a long time, but the dynamics is quite complicated.

Figures 5(a) and (b) show results similar to figures 4(a) and (b) but for a lower pump beam excitation intensity of 0.5 mJ/cm^2/pulse (10^{15} polaritons cm^{-2}). Comparing the contour plots in figures 4 and 5, which are given, using the same scale of grey values, one remarks that the white regions (absorption bleaching and stimulated biexciton emission) have almost disappeared. The lower stimulated biexciton emission leads to a lower density of longitudinal excitons which results in the decrease of the absorption line at 3.186 eV. In addition, the intensity of the ν_2 line is almost constant with time, while it increases with time in figures 4(a) and (b).

If the temperature is raised up to 40 K, the exciton energies increase, which leads to a shift in energy of the induced transmission changes by about 7 meV [36]. The only drastic difference when compared to the features observed at 4 K is a faster recombination dynamics of the free exciton polaritons.

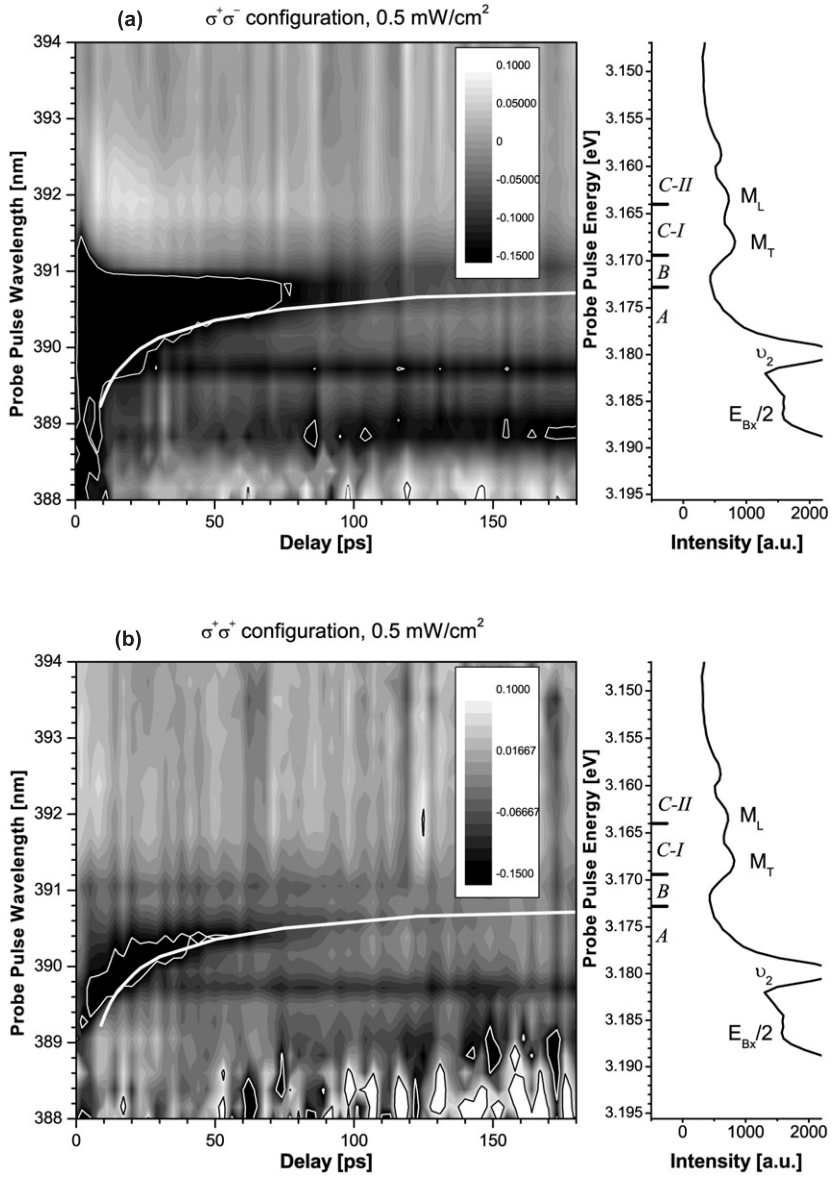

Figure 5. Contour diagram at 0.5 mJ/cm^2/pulse for (a) the $\sigma^+\sigma^-$ configuration and (b) for the $\sigma^+\sigma^+$ configuration.

5. Discussion and modelling of the experimental results

5.1. Modelling of region A (surface effects)

We will discuss in this section the induced transmission changes for several typical photon energies. Figure 2 in [5] is derived from figures 5(a) and (b) for a photon energy of the probe beam $E_t = 3.178$ eV and a low pump pulse intensity (0.5 mJ/cm^2/pulse). The polaritons of the pump pulse which are tested have photon energies $E_p = 3.194$ eV. This figure shows that the quantity $\Delta T^{+-}(t)/T$ for the $\sigma^+\sigma^-$ configuration has its minimum after the end of the

pump pulse and then increases, corresponding to a diminishing of the density of polaritons initially created by the pump pulse. In contrast, the induced transmission change $\Delta T^{++}(t)/T$ for the $\sigma^+\sigma^+$ configuration is equal to 0 at the end of the pump pulse and then decreases. The sum $\Delta T^{+-}(t)/T + \Delta T^{++}(t)/T$ remains almost constant between 0 and a time $t_d = 15$ ps. This indicates that, on this timescale, the main relaxation process is a spin-flip, while the number of polaritons created by the pump pulse is constant. Then, as discussed above, the sum of the transmission changes increases rapidly from a value of about -0.3 to -0.1 after which it remains almost constant. This scenario remains unchanged when pump pulse photons of higher energies (up to 3.1992 eV) or under higher pump pulse excitation are analysed. The main difference is that the drop at t_d happens later and the increase after t_d is slower.

As discussed above, we explain these results by polariton propagation: the polaritons created by the pump pulse propagate almost freely before they arrive at the rear surface of the sample. During the propagation time, these polaritons mainly undergo scattering processes which lead to spin-flip. At the surface, they are either transmitted (and thus lost for the induced absorption of the polaritons from the test pulses) or they are scattered. In the latter case, as shown by the results in figure 2(a) in [5], their spin polarization memory is destroyed.

5.2. Modelling of experimental results for region B (spin-flip region)

The data shown in figure 6(a) are also extracted from figure 5, i.e. they are obtained at a pump beam intensity of 0.5 mJ/cm^2/pulse. As shown in figure 6(a) for $E_t = 3.1715$ eV, the induced absorption dynamics changes drastically if the photon energy of the probe beam is situated in the region $3.1728\ \text{eV} > E_t > 3.1697$ eV. In this region the tested pump-pulse polaritons have photon energies $3.1992\ \text{eV} < E_p < 3.2023$ eV (region B in figure 1). When comparing $\Delta T^{++}(t)/T$ and $\Delta T^{+-}(t)/T$, we nicely see how pump polaritons scatter from σ^+ to σ^- helicity and that their densities become equal at about 150 ps. Then both densities decrease equally with time.

As discussed in more detail in [5], the results can be explained by the following simple model: let us assume that polaritons can either undergo a spin-flip process characterized by the time constant τ_S or scatter to states with higher energies. In this case they are lost for the spin-flip process studied here. If τ_r is the characteristic scattering time constant, the corresponding rate equations are given by

$$\frac{\mathrm{d}N_\pm(t)}{\mathrm{d}t} = -\frac{N_\pm(t)}{\tau_r} - \frac{N_\pm(t)}{\tau_s} + \frac{N_\mp(t)}{\tau_s} \tag{3}$$

where $N_+(t)$ and $N_-(t)$ denote the time-dependent polariton populations with σ^+ and σ^- helicities, respectively. The solutions of the rate equations with the initial conditions $N_+(0) = N_0$ and $N_-(0) = 0$ are

$$N_+(t) + N_-(t) = N_0 \exp(-t/\tau_r) \qquad \text{and} \qquad N_+(t) - N_-(t) = N_0 \exp(-t(1/\tau_r + 2/\tau_s)). \tag{4}$$

In the case of linear absorption changes due to the pump pulses, the test beam transmission in the $\sigma^+\sigma^-$ configuration is given by

$$T^{+-}(t) = I_T/I_{inc} = \exp[-(\alpha_L + N_+(t)\sigma_p)d], \tag{5}$$

where I_{inc} is the intensity of the incident beam, α_L the linear absorption, and σ_p the induced absorption cross-section per polariton. Then,

$$\Delta T^{+-}(t) = (I_{ind}(t) - I_T)/I_T = (\exp[-(N_+(t)\sigma_p)d] - 1). \tag{6}$$

And similarly for $\Delta T^{++}(t)$, replacing $N_+(t)$ by $N_-(t)$.

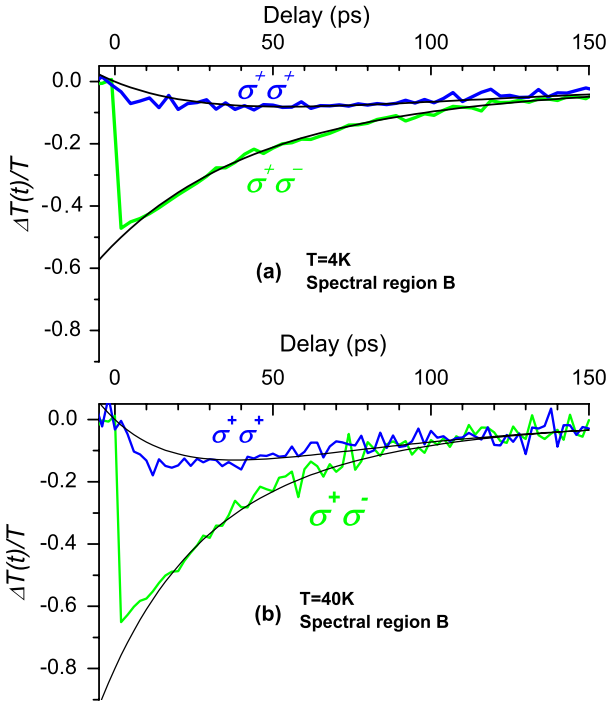

Figure 6. (a) Induced transmission changes for the $\sigma^+\sigma^+$ configuration and for the $\sigma^+\sigma^-$ configuration for $E_t = 3.1715$ eV (corresponding to $E_p = 3.2005$ eV) together with the fit using equation (3). (b) Induced transmission changes for the $\sigma^+\sigma^+$ configuration and for the $\sigma^+\sigma^-$ configuration for $T = 40$ K and $E_t = 3.1777$ eV together with the fit using equation (3).

Figure 6(a) shows the result of the fit of the induced transmission changes with expression (3), and we obtain $\tau_S = 120 \pm 10$ ps and $\tau_r = 80 \pm 10$ ps, respectively. These values remain valid if the excitation intensity remains lower than 1.5 mJ/cm^2/pulse. At higher intensities, the dynamics is faster and a satisfactory fit of $\Delta T^{++}(t)$ and $\Delta T^{+-}(t)$ with our simple model is no longer possible for the results shown in figure 4. Figure 6(b) shows results for the same region but for a temperature of $T = 40$ K and an excitation intensity of 0.5 mJ cm^{-2} pulse^{-1}. We find that τ_S remains unchanged but τ_r decreases to $\tau_r = 60 \pm 10$ ps. This result may indicate that scattering with acoustic phonons becomes important at higher temperatures: such scattering would be mainly inelastic to states with different energies where the polaritons are outside the tested region. If this interpretation is correct, the observed spin-flip time τ_S would be mainly due to elastic scattering with crystal imperfections. As discussed above, this result is compatible with that of region A.

5.3. Modelling of experimental results for region C

The spectral properties of induced absorption again change drastically if the photon energy of the probe beam is situated below $E_t < 3.1694$ eV at 4 K (see figures 4 and 5). In this case the pump-pulse polaritons have photon energies $E_p > 3.2026$ eV, i.e. energies above that of the transverse exciton and inside the polariton bottleneck region (region C in figure 1). Depending on whether the polaritons which are injected into the crystal have energies larger or smaller than the longitudinal exciton, two behaviors are observed.

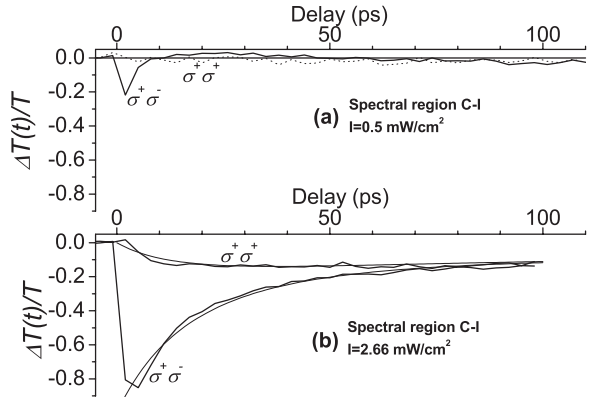

Figure 7. (a) Induced transmission changes for the $\sigma^+\sigma^+$ configuration and for the $\sigma^+\sigma^-$ configuration for $T = 4$ K and $E_t = 3.1654$ eV (corresponding to $E_p = 3.2066$ eV) for 0.5 mJ/cm^2/pulse. (b) Induced transmission changes for the $\sigma^+\sigma^+$ configuration and for the $\sigma^+\sigma^-$ configuration for $T = 4$ K and $E_t = 3.1654$ eV (corresponding to $E_p = 3.2066$ eV) together with the fit using equation (7) for 2.66 mJ/cm^2/pulse.

5.3.1. Region C-I (the polariton bottleneck region). When considering the probe beam photon energy within the region 3.1640 eV $< E_t <$ 3.1694 eV, we probe polaritons created by the pump pulse which have energies in between 3.2080 eV $> E_p >$ 3.2026 eV. The polariton dispersion being almost flat in this region, one obtains a very high density of states. The polaritons show a strong exciton character and this leads to an important scattering rate between polaritons. In figures 7(a) and (b) we show as an example the induced transmission change for $E_t = 3.1654$ eV (corresponding to $E_p = 3.2066$ eV). The data are isolated from figures 5 and 4, i.e. at 0.5 and 2.66 mJ/cm^2/pulse, respectively. At low intensity, besides an induced absorption in the $\sigma^+\sigma^-$ configuration for short delays, no changes can be identified outside the noise level. One sees, however, that the spin memory is nevertheless conserved over longer times for higher intensities of excitations. The absorption dynamics becomes faster when compared to region B, and the densities of polaritons with σ^+ and σ^- helicity become equal earlier, indicating that the spin memory is lost sooner. At this high intensity of excitation, the induced transmission data may be saturated.

Because of the importance of scattering, the model established above is no longer valid in the bottleneck region. We extend it by including biexciton formation similar to [16–18]. The corresponding rate equations are now given by

$$\begin{aligned}
\frac{\mathrm{d}N_T^{\pm}}{\mathrm{d}t} &= +\frac{N_B}{3\tau_B} - \frac{N_T^{\pm}}{\tau_r} - \frac{N_T^{\pm}}{\tau_s} + \frac{N_T^{\mp}}{\tau_s} + \frac{N_L}{2\tau_L} - B_{XX}N_T^{\pm}(N_T^{+} + N_T^{-} + N_L) \\
\frac{\mathrm{d}N_L}{\mathrm{d}t} &= +\frac{N_B}{3\tau_B} - \frac{N_L}{\tau_L} - B_{XX}N_L(N_T^{+} + N_T^{-} + N_L) \\
\frac{\mathrm{d}N_B}{\mathrm{d}t} &= -\frac{N_B}{\tau_B} + \frac{B_{XX}}{2}(N_T^{+} + N_T^{-} + N_L)^2.
\end{aligned} \tag{7}$$

B_{XX}, N_B and τ_B denote the biexciton formation probability through coupling of two excitons, their density, and lifetime, respectively. Biexcitons are created through binding of two excitons, which may be transverse (indices + and −) or longitudinal (index L). It is important to notice that in this relaxation channel (which is mainly achieved through emission of optical phonons followed by biexciton thermalization) the wavevectors and the spin polarizations of the initial excitons are not conserved. The biexcitons dissociate by emitting one photon in the spectral

region of the induced absorption and a longitudinal or transverse exciton. The transition probability to these states is assumed to be the same. In addition, we assume a relaxation of the longitudinal excitons to one of the transverse states, $\tau_L = 130 \pm 10$ ps being the corresponding time constant. The value of τ_L has no significant influence on the results. As shown in figure 7(b) for $T = 4$ K, $E_t = 3.1654$ eV, the induced absorption dynamics can be well explained by this model. We find for the spin-flip times $\tau_s = 70 \pm 10$ ps and transverse exciton lifetimes $\tau_r = 130 \pm 10$ ps, values which are close to those obtained in the B region. The parameters characterizing the biexcitons are $B_{XX} = 10^{-8}$ cm^3 s^{-1} (in close agreement with [17]) and $\tau_B = 120 \pm 10$ ps. It is important to point out that a satisfactory fit of the induced transmission changes cannot be obtained in the frame of the model described by equation (3) (by reducing for example only the spin-flip time). One has to introduce the nonlinear term in order to explain the high values and the fast dynamics of $\Delta T^{++}(t)$ and $\Delta T^{+-}(t)$ which are measured independently. The spin memory is lost through biexciton formation and an increase of the spin-flip probability. The latter is probably due to the high density of states above the polariton bottleneck which favours exciton–exciton scattering processes.

6. Experimental results for region C-II (gain)

If the photon energy of the probe beam is situated below $E_t < 3.1640$ eV at 4 K, the pump-pulse polaritons tested have photon energies $E_p > 3.2080$ eV, which corresponds to energies above that of the longitudinal exciton and above the polariton bottleneck region (region C-II). At this and higher photon energies, depending on the excitation intensity, the system can pass from induced absorption to gain due to induced recombination of biexcitons. As discussed above, biexciton formation is very efficient in CuCl by coupling of two excitons followed by emission of a longitudinal optical phonon. After their recombination, longitudinal excitons are created, which rapidly thermalize to lower states, assuring the population inversion between longitudinal excitons and biexcitons. Figure 8 shows an example of the rapid dynamics for the data from figure 4. They are obtained for $E_t = 3.1594$ eV, corresponding to tested polaritons at energies $E_p = 3.2126$ eV. It is possible to analyse this recombination and thermalization dynamics by rate equations, but the system involves too many parameters to give a significant result.

Figure 8 shows, however, that in this spectral region the spin memory is immediately lost after excitation. This shows up through the fact that induced absorption is only observed in the $\sigma^+\sigma^-$ configuration and if the probe pulse coincides in time with the pump pulse. When the probe pulse is delayed the probe beam is equally amplified in both configurations, independent of its helicity. As described above, in our procedure we have subtracted the stimulated emission due to the pump beam. Compared to this intensity the probe beam is not significantly amplified. This indicates that the stimulated emission builds up from noise immediately after the excitation.

7. Discussion of lifetimes and spin-relaxation times of polaritons

In the spin-flip region, we have found spin-relaxation times $\tau_S = 120 \pm 10$ ps and lifetimes of the polaritons $\tau_r = 80 \pm 10$ ps. In the rate equations (3), we have assumed that spin scattering takes place from σ^+ to σ^- helicity and vice versa. In the following we will discuss this situation, which corresponds to a simultaneous spin-flip of the electron and the hole (as can be induced for example by electron–hole exchange interaction using the Bir, Aronov and Pikus mechanism [37]) but not to a single particle effect as for example the mechanism named

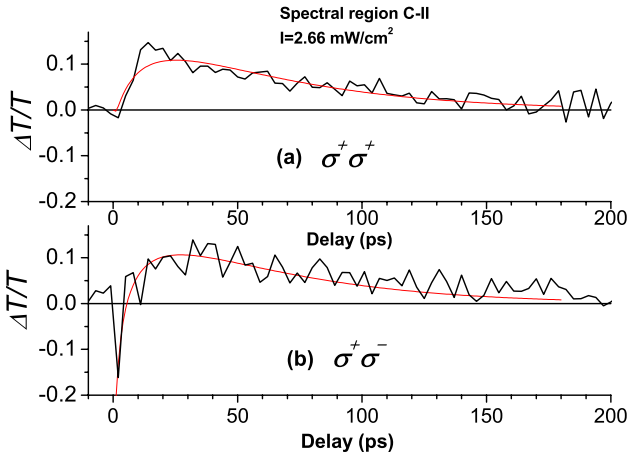

Figure 8. Induced transmission changes for the $\sigma^+\sigma^+$ configuration (a) and for the $\sigma^+\sigma^-$ configuration (b) for $T = 4$ K and $E_t = 3.1594$ eV (corresponding to $E_p = 3.2126$ eV) for 2.66 mJ/cm^2/pulse.

after D'yakonov and Perel [38]. As discussed in the introduction, in CuCl, the valence and the conduction bands are only twofold degenerated and the product space of electron and hole states can be described by Pauli spin-1/2 matrices. Let α_i and β_i denote the spin up and down states of the electrons ($i = \mathrm{e}$) and holes ($i = \mathrm{h}$), respectively. Then, the optical active exciton states with σ^+ to σ^- helicities (noted +1 and −1) are proportional to the product

$$|+1\rangle = |\alpha_\mathrm{e}\rangle|\alpha_\mathrm{h}\rangle \qquad \text{and} \qquad |-1\rangle = |\beta_\mathrm{e}\rangle|\beta_\mathrm{h}\rangle. \tag{8}$$

The optically inactive states are the exciton state with Γ_2 symmetry (denoted 0) and the longitudinal exciton state with Γ_5 symmetry (denoted L) are given by

$$|0\rangle = \frac{1}{\sqrt{2}}(|\alpha_\mathrm{e}\rangle|\beta_\mathrm{h}\rangle + |\beta_\mathrm{e}\rangle|\alpha_\mathrm{h}\rangle) \qquad \text{and} \qquad |L\rangle = \frac{1}{\sqrt{2}}(|\alpha_\mathrm{e}\rangle|\beta_\mathrm{h}\rangle - |\beta_\mathrm{e}\rangle|\alpha_\mathrm{h}\rangle). \tag{9}$$

This situation is very different from the one which occurs in semiconductor quantum wells where spin-flip processes have been largely studied (see for example [39]). As discussed in the introduction, only the transverse exciton states and the resulting polariton dispersions are degenerate in energy. Therefore, quasi-elastic scattering is possible if the electron and the hole change their spin state simultaneously and pass from one optical active state to the other. This is measured by the spin-relaxation time τ_S.

In the absence of external fields, as given in detail in [12], an intrinsic exchange interaction breaks the symmetry of the Hamiltonian which it has at the Γ-point. This symmetry breaking effect depends on the exciton wavevector Q and acts as an effective magnetic field around which the total angular momentum of the polariton precesses. If in a scattering process the wavevector changes, the effective field changes its magnitude and direction, leading to spin relaxation of the polaritons. Since the electron–hole exchange interaction is diagonal at the Γ point, the leading term is proportional to Q^2. In low symmetry directions electron–hole exchange interaction can even lead to a wavevector-dependent lifting of the degeneracy of the polariton branches, but this splitting remains very small [12]. In the spin-flip region Q is typically 4×10^5 cm^{-1} and about 10 times bigger in the bottleneck region. This may explain the dependence of τ_S on the photon energy: we can fit our results in regions B and C-I with values of τ_S which are different but of the same order of magnitude. Since, in addition, τ_S is independent of temperature in the spin-flip region, we believe that the exciton spin-flip is due

to scattering with crystal imperfections and partly due to electron–hole exchange but not to phonons which rather contribute in inelastic scattering processes leading to a decrease of the polariton density in the studied region.

If a spin-flip takes place only for an electron or a hole, a superposition of a longitudinal Γ_5 and a Γ_2 exciton states is created. Using the invariant expansion of the Hamiltonian for this process [12], the leading term would be proportional to Q^3. Such processes could influence τ_L but do not show up directly in our measurements since only dark exciton states are involved in the process. In the spin-flip region and the lower part of the bottleneck region this is only possible for inelastic scattering processes, because the longitudinal–transverse splitting is different from the singlet–triplet splitting. Concerning τ_L, we therefore believe that it is mainly limited by non-radiative recombination of electron–hole pairs and perhaps influenced by inelastic scattering with phonons at higher temperatures.

8. Conclusion

We have studied the time evolution of the total angular momentum (or pseudo-spin) of polaritons. We have shown that the spin-flip time and the relaxation dynamics of exciton polaritons can be determined by non-degenerate induced-absorption measurements. We have measured the variation of the population and spin dynamics as a function of the wavevector, going from fast to slow polaritons, for which the larger collision probability gives rise to a complex nonlinear dynamics in the biexciton–exciton system.

- When polaritons are created at low energies, their slight photon character makes their group velocity very high. They very quickly reach the rear side of the sample where they lose their spin if they are scattered back.
- When approaching the polariton bottleneck at higher photon energies, there is a small spectral region where their spin dynamics, related to their strong exciton character, can be measured. Their group velocity is reduced enough to increase the time the polaritons live in the sample and to make the whole spin relaxation observable.
- For even higher photon energies, directly in the bottleneck, the polaritons are fully excitons and, moreover, their density of states becomes very high because their group velocity is reduced by a few orders of magnitude. In this region, polariton–polariton collision processes become the dominant dephasing mechanisms, leading to a more complex dynamics depending on the excitation intensity, where the biexciton and longitudinal exciton levels are populated. Gain can be observed between these latter states, if the excitation occurs above the longitudinal exciton energy. In the whole spectral region, the absence of spin conservation during these processes induces a very short spin dynamics.

Concerning the exciton spin relaxation mechanisms, we have shown the following.

- Polaritons scattered back from a sample surface lose their spin.
- Spin relaxation of excitons is dominated by collisions with crystal imperfections, more than by electron–hole exchange interaction and not by collision with phonons.
- Inside the bottleneck region but not in the spin-flip region, the biexciton formation process is very efficient at randomizing the spin of the polariton population.

Our non-degenerate pump-and-probe technique allow thus following the spin memory of exciton polaritons. It is very promising for the study of other systems which obey to the same type of selection rules for two polariton transitions. This is probably the case in confined semiconductors.

References

[1] For recent reviews see
Prinz G 1995 *Phys. Today* **48** 58
Prinz G 1998 *Science* **282** 1660
DiVincenzo D P 1995 *Science* **270** 255
Wolf A, Awschalom D D, Buhrman R A, Daughton J M, von Molnàr S, Roukes M L, Chtchelkanova A Y and Treger D M 2001 *Science* **294** 1488 and references cited therein
[2] Ohno H, Matsukura F and Ohno Y 2002 *JSAP Int.* **5** 4
[3] Adachi S, Miyashita T, Takeyama S, Takagi Y, Tackeuchi A and Nakayama M 1997 *Phys. Rev.* B **55** 1654
[4] Snoke D W, Rühle W W, Köhler K and Ploog K 1997 *Phys. Rev.* B **55** 13789
[5] Rahimpour Soleimani H, Cronenberger S, Crégut O, Likformann J-P, Gallart M, Ostatnický T, Gilliot P and Hönerlage B 2004 *Appl. Phys. Lett.* **85** 5263
[6] Mann Ch, Langbein W, Woggon U and Ivanov A L 2001 *Phys. Rev.* B **64** 235206
[7] White T H K, Birch J A and White G K 1977 *J. Phys. C: Solid State Phys.* **10** 1617
[8] Reimann K and Rübenacke St 1994 *Phys. Rev.* B **49** 11021
[9] Raga F, Kleim R, Mysyrowicz A, Grun J B and Nikitine S 1967 *J. Physique Coll.* **28** C3 116
[10] Göbel A, Ruf T, Lin Ch T, Cardona M, Merle J-C and Joucla M 1997 *Phys. Rev.* B **56** 210
[11] Fröhlich D, Kohler P, Nieswand W and Mohler E 1991 *Phys. Status Solidi* b **167** 147
[12] Hönerlage B, Lévy R, Grun J B, Klingshirn C and Bohnert K 1985 *Phys. Rep.* **124** 161 and references cited therein
[13] Hönerlage B, Bivas A and Phach V D 1978 *Phys. Rev. Lett.* **41** 49
[14] Phach V D, Bivas A, Hönerlage B and Grun J B 1978 *Phys. Status Solidi* b **86** 159
[15] Grun J B, Hönerlage B and Lévy R 1982 *Exciton* vol 2, ed E I Rashba and M D Sturge (Amsterdam: North-Holland) p 459 and references cited therein
[16] Lévy R, Hönerlage B and Grun B 1979 *Solid State Commun.* **29** 103
[17] Lévy R, Hönerlage B and Grun B 1979 *Phys. Rev.* B **19** 2326
[18] Gomes M J M, Lévy R and Hönerlage B 1991 *J. Lumin.* **48/49** 83
[19] Leonelli R, Manar A, Grun J B and Hönerlage B 1992 *Phys. Rev.* B **45** 4141
[20] Akiyama H, Kuwata M, Kuga T and Matsuoka M 1989 *Phys. Rev.* B **39** 12973
[21] Akiyama H, Kuga T, Matsuoka M and Kuwata-Gonokami M 1990 *Phys. Rev.* B **42** 5621
[22] Kuwata-Gonokami M, Shimano R, Iwamatsu J, Akiyama H, Kuga T and Matsuoka M 1990 *Phys. Status Solidi* b **159** 347
[23] Ikehara T and Itoh T 1991 *Solid State Commun.* **79** 755
[24] Kurihara K, Tokunaga E, Baba M and Matsuoka M 1995 *Phys. Rev.* B **52** 8179
[25] Masumoto Y, Unuma Y, Tanaka Y and Shionoya S 1979 *J. Phys. Soc. Japan* **47** 18844
[26] Bassani F, Forney J J and Quattropani A 1974 *Helv. Phys. Acta* **47** 20
Bassani F, Forney J J and Quattropani A 1974 *Phys. Status Solidi* b **65** 591
Hanamura E 1975 *J. Phys. Soc. Japan* **39** 1516
[27] Phach V D, Bivas A, Hönerlage B and Grun J B 1977 *Phys. Status Solidi* b **84** 731
[28] Ivanov A L, Hasuo M, Nagasawa N and Haug H 1994 *Phys. Rev.* B **52** 11017
[29] Hasuo M, Nishino M and Nagasawa N 1994 *J. Lumin.* **60/61** 672
[30] Vanagas E, Kudrna J, Brinkmann D, Gilliot P and Hönerlage B 2001 *Phys. Rev.* B **63** 153201
Levy R, Gomes M J M, Kippelen B and Hönerlage B 1990 *Phys. Status Solidi* b **158** 391
[31] Hasuo M, Kawano H and Nagasawa N 1995 *Phys. Status Solidi* b **177** 77
Kuwata M and Nagasawa N 1983 *Solid State Commun.* **45** 937
[32] Ivanov A L, Haug H and Keldysh L V 1998 *Phys. Rep.* **296** 237 and references cited therein
[33] Ichimiya M, Watanabe M and Hayashi T 2001 *Phys. Status Solidi* b **228** 847
[34] Levy R and Grun J B 2001 *Phys. Status Solidi* a **228** 847
Certier M, Wecker C and Nikitine S 1969 *J. Phys. Chem. Solids* **30** 1281
[35] Adachi S, Miyashita T, Takeyama S, Takagi Y, Tackeuchi A and Nakayama M 1997 *Phys. Rev.* B **55** 1654
[36] Levy R, Klingshirn C, Ostertag E, Phach V D and Grun J B 1976 *Phys. Status Solidi* b **77** 381
[37] Bir G L, Aronov A G and Pikus G E 1975 *Sov. Phys.—JETP* **42** 705
[38] D'yakonov M I and Perel V I 1972 *Sov. Phys.—Solid State* **13** 3023
[39] Maialle M Z, de Andrada e Silva E A and Sham L J 1993 *Phys. Rev.* B **47** 15776